Applied Thermal Engineering 201 (2022) 117844

Contents lists available at ScienceDirect

Applied Thermal Engineering

journal homepage: www.elsevier.com/locate/apthermeng

A detailed energy analysis of a novel evaporator with latent thermal energy storage ability

Boniface Dominick Mselle , Gabriel Zsembinszki , David Vérez , Emiliano Borri , Luisa F. Cabeza *

GREiA Research Group, Universitat de Lleida, 25001 Lleida, Spain

ARTICLE INFO

Keywords:
Energy analysis
Thermal energy storage (TES)
Phase change materials (PCMs)
Heat exchange
Experimental study

ABSTRACT

The direct integration of phase change materials (PCM) into refrigeration and air conditioning systems through compact modules is an identified literature gap. In response to the literature gap, this paper provides a detailed energy analysis of a novel compact thermal energy storage module, that allows its direct integration into a refrigeration system as the evaporator. The study addresses key aspects of thermal energy storage (TES) and heat transfer mechanism that complement the previous analyses of the novel concept. Here the total energy stored in the module (including in all auxiliary parts), the charging/discharging power, and the behaviour of the module when used as a TES module and as a heat exchanger (HEX) are assessed. The results demonstrate the feasibility of the module to work as a TES and as a HEX. When working as a TES, complete charging and discharging was achieved, and 54% of the total energy was stored in the PCM although the PCM only accounts for around 14% of the total mass. Moreover, the highest charging/discharging power was obtained within the temperature range where most of the phase change occurred. When the module works as a HEX, it initially charges/discharges partially until a thermal equilibrium is achieved and the level of charge responds to the variation in the energy supply and demand.

1. Introduction

Over years, there is an increased motivation to use renewable energy sources over fossil fuels to respond to global climate change and to encourage sustainable development [1–4]. The technologies intended to take advantage of renewable energy sources rely on energy storage systems to balance the mismatch between energy supply and energy demand profiles. For thermal energy storage (TES), an interesting option is the use of phase change materials (PCM) as a storage medium, which are characterised by high energy storage density and near-isothermal energy release/absorption during the phase change [5]. The high energy storage density enables the construction of more compact TES systems that require less space, while their ability to absorb/release energy at relatively constant temperature encourages their incorporation into various technologies [6].

The design of a TES system determines the overall energy storage density and the ability to respond to the energy demand and supply [6]. One of the designs that is gaining more interest due to its potential in a wide range of applications, both in buildings and industrial sectors, is the inclusion of PCM into heat exchangers [7–9]. Several aspects were studied from lab-scale to pilot-plant-scale. Medrano et al. [10] experimentally assessed the rate of heat transfer of five lab-scale commercial PCM heat exchangers, reporting the temperature evolution and thermal power of the PCM. Gasia et al. [11] studied the thermal behaviour of a pilot plant-scale shell-and-tube heat exchanger with a commercial paraffin as PCM for waste heat recovery reporting non-linearity in the energy storage and release by the PCM. Zsembinszki et al. [12] carried out an experimental study on a lab-scale heat exchanger for cooling applications filled with a commercial PCM, analysing different techniques to determine the state-of-charge of the PCM, reporting the best approach as a combination of two or more techniques.

All designs aforementioned allow heat exchange between PCM and liquid HTF, and there are very few studies considering the use of the refrigerant as the HTF in PCM charging/discharging. A techno-economic analysis was performed in [13], on the integration of a refrigerant-PCM-water heat exchanger into an air-source heat pump, reporting a favourable economic performance for such internal heat exchangers, especially in low temperature ranges below 50 K. Varvagiannis et al.

* Corresponding author.
E-mail addresses: boniface.mselle@udl.cat (B.D. Mselle), gabriel.zsembinszki@udl.cat (G. Zsembinszki), david.verez@udl.cat (D. Vérez), emiliano.borri@udl.cat (E. Borri), luisaf.cabeza@udl.cat (L.F. Cabeza).

https://doi.org/10.1016/j.applthermaleng.2021.117844
Received 18 February 2021; Received in revised form 24 September 2021; Accepted 21 November 2021
Available online 24 November 2021

[14] numerically investigated the replacement of an evaporator of a conventional chiller by a novel refrigerant-PCM-water heat exchanger in a hybrid electrical and thermal storage system. The study identified an enhanced solar fraction when using the novel heat exchanger. Moreover, Mselle et al. [15] performed a parametric study of a novel refrigerant-PCM-water heat exchanger reporting the system boundary conditions for the charging and discharging of the PCM. The study was considered a preliminary analysis of the novel concept of a refrigerant-PCM-water heat exchanger. Nevertheless, the studies aforementioned tend to focus only on the charging and discharging of the PCM, missing to include the energy storage in the sensible material, the heat/cold losses in the piping system, and the losses due to the mechanical efficiencies of components in the systems.

Given the identified literature gap, this paper experimentally studies a novel evaporator that would replace the conventional evaporator of a refrigeration system. The evaporator is a refrigerant-PCM-water heat exchanger that was designed to allow heat exchange among the three fluids. The study on the novel concept was reported for the first time by the same authors using a similar module in a previous paper in [15], where preliminary results and the optimum operating conditions in charging and discharging of the PCM were reported. In this paper, a step beyond the previous study is covered, analysing the total energy stored in the module (including the energy stored in all the auxiliary parts), the heat transfer rate (power) in the PCM, in the sensible material, and in the whole module, and also the cold power delivered to the external loop (HTF loop). Moreover, the behaviour of the module is assessed when used as a TES device and as a HEX to demonstrate and discuss the feasibility to use it both as a TES device and as a HEX. Moreover, the variations of energy and power are quantified, especially when boundary conditions are changing, showing the response of the module when a change in the energy supply or the energy demand occurs. Indeed, these are key aspects to study in such a novel module to assess its potential and portray any room for further improvements. Finally, an experimental assessment of the heat loss and uncertainty in the results are included.

2. Materials and methods

2.1. Description of the novel evaporator-TES module

The device investigated in this study is a novel lab-scale evaporator-TES module developed by AKG (Germany), with four PCM layers sandwiched between the refrigerant and the HTF (water-glycol mixture) channels. Such channels distribution allows simultaneous processes of thermal energy storage and heat transfer between the refrigerant and the HTF.

The module is made of dip-brazed aluminium and it is intended to be used as a thermal energy storage and a heat exchanger in cooling applications. To meet the design requirements, the module consists of seven rectangular blocks, i.e. the central part (A) of the module, where most of the heat transfer takes place, one distributor for the HTF (W1), and one for the refrigerant (R1), one collector for the HTF (W2) and one for the refrigerant (R2), and two PCM storage containers (P1 and P2), as seen in Fig. 2. The central part is designed in such a way to increase the surface area of heat exchange among the refrigerant, PCM, and the HTF, while the distributors are designed to distribute and direct the flow of the fluids. The two PCM storage containers are included to provide more space for the PCM and the collectors enable depositing the fluids as they leave the module. The location and dimensions of the blocks are presented in Fig. 1; block A (300 × 94 × 310 mm), block W1 and W2 (60 × 94 × 310 mm), block R1 and R2 (45 × 55 × 310 mm), and block P1 and P2 (65 × 55 × 310 mm). Moreover, the module was insulated with 120-mm-thick rock wool. To enable the evaluation of the energy storage in each material consisted in the TES module, all the materials were weighted, obtaining the weight of the empty module as $m_{Al} = 20.38$ kg, that of the HTF in the module as 3.26 kg, and that of the PCM as 3.70 kg.

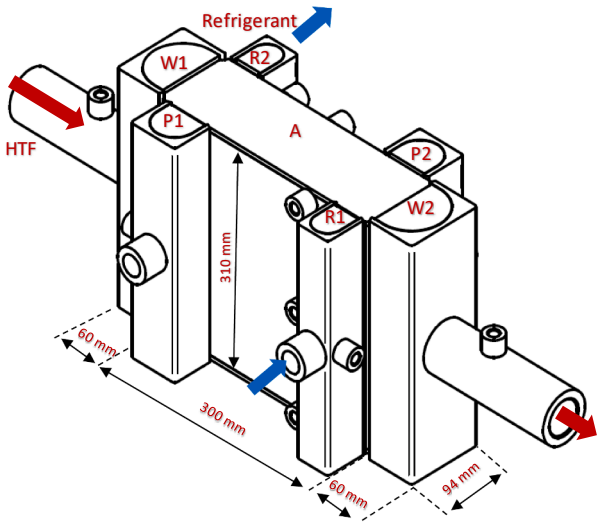

Fig. 1. The external dimensions of the evaporator-TES module (AKG-Germany).

2.2. Materials and characterization

The commercial RT4 PCM used for the latent energy storage is an organic paraffin, chemically inert, and thermally stable. According to the manufacturer [16], some of the thermophysical properties of the PCM are (Table 1): thermal conductivity of 0.2 $W{\cdot}m^{-1}{\cdot}K^{-1}$, phase change temperature ranging from 2 °C to 4 °C, density ranging from 880 $kg{\cdot}m^{-3}$ in solid state to 770 $kg{\cdot}m^{-3}$ in liquid state, and volume expansion of about 12.5%.

Due to the need for accurate thermophysical properties of the PCM, the specific heat capacity and the phase change enthalpy were experimentally tested using a DSC 3+ Mettler Toledo equipment with ±0.1 K precision for temperature and ±3 $J{\cdot}s^{-1}$ for enthalpy. The amount of sample used was around 10 mg and experiments were performed under N_2 flow. The PCM samples were located into 100 μL cold-welded aluminium crucibles. The melting and solidification enthalpy were tested with a dynamic programme, heating the sample from −22 °C to 22 °C at 10 $K{\cdot}min^{-1}$. Each sample was cycled three times, disregarding the first one [17]. The specific heat capacity was determined with the method developed by Ferrer et al. [18], performing three measurements for each sample, a blank measurement, a reference material measurement (with sapphire), and the tested material measurement. Another material that contributes to energy storage inside the TES is the HTF itself that occupies part of the internal volume. The HTF is a mixture of 70% water and 30% glycol. The thermophysical properties of the HTF according to the manufacturer [19] are as follows: freezing temperature at −18 °C, an average density of 1050.45 $kg{\bullet}m^{-3}$, an average specific heat of 3601.5 $J{\bullet}kg^{-1}{\bullet}K^{-1}$, and an average thermal conductivity of 0.4275 $W{\bullet}m^{-1}{\bullet}K^{-1}$ in the temperature range between 12 °C and −4 °C. To obtain the sensible energy stored in the aluminium structure, the value for the specific heat capacity of aluminium of 900 $J{\bullet}kg^{-1}{\bullet}K^{-1}$ from the literature [20] was used.

2.3. Experimental set-up

The module was installed in a dedicated experimental set-up, shown in Fig. 2, built in the laboratory of GREiA research group at the Universitat de Lleida, in Spain. The set-up consists of two loops: the refrigerant loop that supplies the cold energy to the module, and the HTF loop that discharges the cold energy from the module. The refrigerant loop consists of a condensing unit (Zanotti model GCU2030ED01B) able to work at different operation powers, working with R449A refrigerant

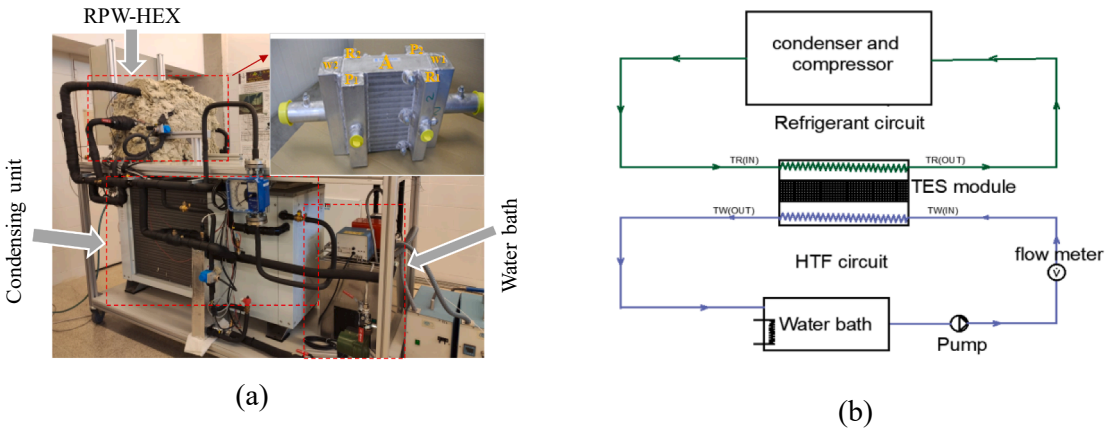

Fig. 2. (a) The novel module directly integrated into the refrigeration system and the HTF loop; (b) the schematic diagram of the experimental set-up.

Table 1
Properties of the commercial RT4 PCM [16].

Properties	Value	Units
Phase change range	2–4	°C
Density	0.88 (solid) 0.77 (liquid)	kg·L^{-1}
Thermal conductivity	0.2	W·m^{-1}·K^{-1}
Volume expansion	12.5	%

and containing a hermetic scroll compressor (CU E scroll digital); an electronic expansion valve; and an air-cooled condenser. According to the manufacturer, the condensing unit has a maximum power of 4.956 kW with a COP of 2.12 when operating at evaporation temperature of −10 °C and ambient at 32 °C. The HTF circuit is built to ensure a stable inlet temperature into the module by incorporating two immersion electric heaters (OVAN TH100E-2 kW and JP SELECTA-1 kW) and two immersion chillers (JP SELECTA FRIGEDOR-285 W) into a water bath. Moreover, the circuit contains a pump for circulation and an advanced flow meter (Badger Meter Primo) with an accuracy of ±0.25%.

A total of 13 temperature sensors (Pt-100 class B, IEC 60751 standard type) with an accuracy of ±0.3 °C connected to a data acquisition system (STEP DL-01 data logger) were used to record the experimental measurements every 10 s into a computer with Indusoft SCADA software. To capture the temperature at different positions in the module, nine of the temperature sensors were distributed evenly in the module such that they were in direct contact with the PCM, as shown in Fig. 3. To maximize the accuracy of the theoretical calculations based on the temperature measurements, the sensors were located as widely as possible and following symmetry criteria. The rest of the temperature sensors were installed at each inlet and outlet of the two loops. The module was insulated with a 12-cm-thick rock wool material to reduce the heat losses to the ambient.

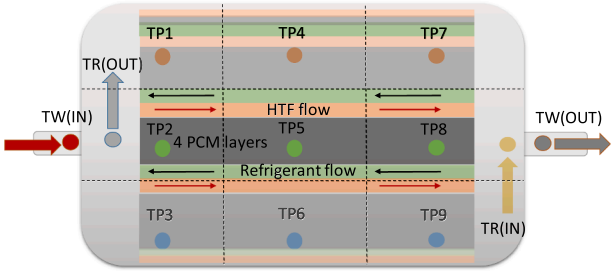

Fig. 3. Position of the temperature sensors.

2.4. Experimental methodology

The design of the experimental set-up allowed testing the module in various boundary conditions simulating the energy demand and the energy source. In the first case, the module was initially at (12 ± 0.5) °C (meaning that it was completely discharged, i.e. the PCM was in liquid state) and a constant energy source level was maintained at different levels of energy demand. This was achieved by performing several experiments at constant 30% compressor power, (12 ± 0.5) °C HTF inlet temperature, and different HTF flow rates (Case 1 in Table 2).

In the second case, the influence of different levels of energy source was assessed by performing several experiments at different compressor powers with the module initially at (−4 ± 0.5) °C (meaning that it was completely charged, i.e. the PCM was fully solidified), while maintaining the HTF inlet conditions at (12 ± 0.5) °C and 100 L·h^{-1} (Case 2 in Table 2). Before starting any experiment, the module, the water bath, and the condensing unit were set to the required experimental conditions, and to ensure repeatability and robustness of the results, at least three repetitions were performed.

Moreover, the overall UA value of heat losses of the module was experimentally estimated from a heat loss test. To do this, the module was completely charged to −4 °C, then allowed to discharge by heat transfer from the ambient air until it reached an average temperature around 12 °C. To ensure that the energy loss was only through heat transfer from the ambient at the surface of the module, all the valves were closed to stop any flow through the module.

Furthermore, an experiment was performed to assess the validity of the discrete volume approach described in the next section. To realize this, the module was charged using compressor power at 25% until all the PCM in the module was completely charged beyond −4 °C and then stopped, after which the HTF was immediately allowed to flow at 12 °C and 100 L·h^{-1} through the module to discharge the cold energy. The validity of the discrete volume approach was assessed using the HTF loop because of its reliability in terms of the accuracy of thermophysical properties and HTF flow rate measurements.

Table 2
Set of experiments.

	Compressor power [%]	HTF flow rate [L·h^{-1}]	Module initial temperature [°C]
Case 1	30	0, 50, 100, 150	12 ± 0.5
Case 2	0, 15, 20, 25, 30	100	−4 ± 0.5

2.5. Theoretical evaluation methodology

To estimate the energy stored in the module, the discrete volume approach in [21–23] was adapted. In this study, the approach was used to divide the module into nine small volumes/nodes with respect to the nine temperature sensors in contact with the PCM (Fig. 3). Then the energy stored in the module was evaluated from the temperature, the specific heat capacity, and the mass of the material in each volume/node. The approach was used to enable a more accurate energy assessment, by evaluating the mass of each material contributing to energy storage in each volume element, i.e. PCM, aluminium (Al), and HTF inside the module. Basic equations on energy balance and heat transfer, Eqs. (1)–(11) obtained from Cengel and Boles [24] were applied in the evaluation. The following assumptions were made: the temperature of the PCM, aluminium, and HTF was uniform at each node, the solidification of the PCM was homogenous and continuous, the PCM was evenly distributed and there was no flow during PCM phase change, so the mass of the PCM inside each volume element of the module remained constant regardless of the state of the PCM during the phase change process, and the thermocouples did not affect the flow field of the experimental device.

The amount of energy stored in the PCM at every time instant, E_{PCM}, was evaluated as the sum for all volume elements of the product between the PCM mass in volume element i, $m_{PCM,i}$, and the PCM specific enthalpy, $h_{PCM,i}$, as shown in Eq. (1):

$$E_{PCM} = \sum_{i=1}^{n} m_{PCM,i} \cdot h_{PCM,i} [kJ] \tag{1}$$

where the specific enthalpy of the PCM in a specific volume i depends on the value of the temperature measured by the sensor located in that volume.

Likewise, the amount of energy stored in the HTF, E_{HTF}, was obtained using Eq. (2), as the sum of all volume elements of the product between the HTF mass in each volume element, $m_{HTF,i}$, the specific heat capacity of the HTF, Cp_{HTF}, and the temperature difference between the reference temperature (12 °C) and the HTF temperature, $T_{HTF,i}$:

$$E_{HTF} = \sum_{i=1}^{n} m_{HTF,i} \cdot Cp_{HTF} \cdot (12 - T_{HTF,i}) [kJ] \tag{2}$$

Similarly, the amount of energy stored in the aluminium was obtained as the sum for all volume elements of the product between its mass, m_{Al}, specific heat capacity, Cp_{Al}, and the temperature difference between the reference temperature (12 °C) and the Al temperature, as shown in Eq. (3):

$$E_{Al} = \sum_{i=1}^{n} m_{Al,i} \cdot Cp_{Al} \cdot (12 - T_{Al,i}) [kJ] \tag{3}$$

The temperature of the HTF ($T_{HTF,i}$) and aluminium ($T_{Al,i}$) in volume element i used in Eqs. (2) and (3), respectively, was assumed to be equal to the temperature of the PCM in the same volume element (i.e. the temperature measured by the sensor located in the volume element i).

To obtain the total amount of energy stored in the module, E_{TES}, during each process, the sum of the contribution from each material was performed as in Eq. (4):

$$E_{TES} = E_{PCM} + E_{HTF} + E_{Al} [kJ] \tag{4}$$

The validity of the discrete volume approach was assessed using the law of energy conservation, according to which the total energy discharged from the module, $E_{discharged}$, should be equal to the sum of the energy delivered to the HTF, E_{HTF}, and the energy lost to the ambient, E_{losses}, as shown in Eq. (5):

$$E_{discharged} = E_{HTF} + E_{losses} [kJ] \tag{5}$$

where the total energy discharged through the HTF (E_{HTF}) was calculated as the sum of the product between the HTF power, $\dot{E}_{HTF}$, and the time step between registered data over the whole discharging process. The power transferred to the HTF loop, $\dot{E}_{HTF}$, was calculated as the product of the HTF specific heat capacity, Cp_{HTF}, mass flow rate $\dot{m}_{HTF}$, and the difference between the inlet temperature, $T_{HTF,in}$, and the outlet temperature, $T_{HTF,out}$, as shown in Eq. (6):

$$\dot{E}_{HTF} = \dot{m}_{HTF} \cdot Cp_{HTF} \cdot (T_{HTF,in} - T_{HTF,out}) [kW] \tag{6}$$

The power transferred to the module, $\dot{E}_{TES}$, was calculated as the variation of the total energy stored in the module, E_{TES}, during a given time interval, Δt, as shown in Eq. (7):

$$\dot{E}_{TES} = \frac{\Delta E_{TES}}{\Delta t} [kW] \tag{7}$$

Similarly, the power transferred to the PCM, $\dot{E}_{PCM}$, was calculated as the variation of the total energy stored in the PCM, E_{PCM}, during a given time interval, Δt, as shown in Eq. (8):

$$\dot{E}_{PCM} = \frac{\Delta E_{PCM}}{\Delta t} [kW] \tag{8}$$

To estimate the energy lost to the ambient, E_{losses}, the overall UA value of the module was experimentally estimated using Eq. (9):

$$UA = \frac{E_{losses}}{\Delta t \cdot \Delta T_{ln}} \left[W \cdot K^{-1} \right] \tag{9}$$

where E_{losses} is the total energy variation of the module due to the energy losses and Δt is the time (in seconds) needed for the TES to heat from −4 °C to 12 °C. The logarithmic mean temperature difference, ΔT_{ln}, is the average temperature difference between the module, $T_{avg,TES}$, and the ambient air, T_a, along the whole process, and it was experimentally evaluated using Eq. (10):

$$\Delta T_{\ln} = \frac{(T_a - T_{avg,TES})_i - (T_a - T_{avg,TES})_f}{In\left(\frac{(T_a - T_{avg,TES})_i}{(T_a - T_{avg,TES})_f}\right)} [^{\circ}C] \tag{10}$$

where a subscript i and f refers to the values at the initial and final point of the process, respectively.

The estimated UA value was then considered in each process to evaluate the rate of heat losses at any time instant t, $\dot{E}_{losses,t}$, according to Eq. (11):

$$\dot{E}_{losses,t} = UA \cdot \Delta T_{\ln,t} [kW] \tag{11}$$

To ensure the accuracy of the results, an analysis of the uncertainty was carried out as shown in Eq. (12), taking into account the contribution from the measurements of the temperature (Pt-100 with an accuracy of ±0.3 °C), the volumetric flow rate given as 0.3% by the manufacturer, the density of HTF as 0.31% from [25], and the specific heat capacity as 3.09% from [26]). The uncertainty was evaluated for normal probability distribution according to the GUM methodology [27], a methodology exemplified in [28].

$$u(\dot{E}_{HTF}) = \left[\left[\frac{\delta \dot{E}}{\delta \rho} u(\rho_{HTF}) \right]^2 + \left[\frac{\delta \dot{E}}{\delta \dot{V}} u\left(\dot{V}_{HTF} \right) \right]^2 + \left[\frac{\delta \dot{E}}{\delta \mathrm{Cp}} u(Cp_{HTF}) \right]^2 + \left[\frac{\delta \dot{E}}{\delta \Delta T_{HTF}} u(\Delta T_{HTF}) \right]^2 \right]^{0.5} \tag{12}$$

where $u(\rho_{HTF})$ is the uncertainty in the density, $u\left(\dot{V}_{HTF}\right)$ is the uncertainty in the volumetric flow, $u(Cp_{HTF})$ is the uncertainty in the specific heat capacity, and $u(\Delta T_{HTF})$ is the uncertainty in the temperature measurements. For the experimental results provided, the expanded relative uncertainty for $u(\dot{E}_{HTF})$ (at 95% confidence level and normal probability distribution, with = 2) was estimated as 4.6%.

3. Results and discussions

3.1. Materials characterization

The amount of cold energy stored in the PCM as it solidified from 12 °C (zero reference enthalpy) to −4 °C strongly depends on the specific enthalpy curve of the PCM within this temperature range. Based on the results obtained from DSC measurements for the PCM performed in the lab, for both the phase change and sensible temperature ranges, the relation shown in Eq. (13) was used to obtain the specific enthalpy of the PCM as a function of its temperature [15]:

$$\begin{cases} h_i = 152.49 + 2.64\cdot(-4 - T_i)[kJ\cdot kg^{-1}], if\, T_i < -4^{\circ}C \\ h_i = -0.1139\cdot T_i^3 + 1.3116\cdot T_i^2 - 8.5545\cdot T_i + 131.97[kJ\cdot kg^{-1}], if\, -4^{\circ}C \le T_i < 6^{\circ}C \\ h_i = -0.0985\cdot T_i^3 + 2.8732\cdot T_i^2 - 28.629\cdot T_i + 99.839[kJ\cdot kg^{-1}], if\, 6^{\circ}C \le T_i \le 12^{\circ}C \\ h_i = -2.38\cdot(T_i - 12)[kJ\cdot kg^{-1}], if\, T_i > 12^{\circ}C \end{cases} \quad (13)$$

where, h_i is the 'cold' specific enthalpy of the PCM and T_i is the temperature of the PCM in the volume element i at any time instant.

3.2. Validity check

Fig. 4 presents the heat loss test performed to estimate the UA value. The experiment started with the module completely charged at −4 °C and was left to heat up to 12 °C only by heat transfer from the ambient. Moreover, the test started with the module charged with around 1000 kJ of cold energy, and the energy level decreased to zero in 16.5 h, registering a heat loss average power of 17.3 W. The mean temperature between ambient temperature (22 °C) and the average temperature of the module (ΔT_{ln}) was evaluated as 17.8 °C. Using Eq. (9), the UA value was evaluated as 0.978 $W\cdot K^{-1}$, which was used to determine heat losses throughout all the experimental tests shown in this paper.

Fig. 5 shows the results of the experiment performed to assess the validity of the discrete volume approach. From the temperature evolution presented in Fig. 5a, it can be observed that the PCM was allowed to completely charge beyond −4 °C before switching to the discharging process. For clarity and better visualization, the results of the temperature evolution are presented in terms of the mean weighted values as T_avg_top for sensors located at the top (TP1, TP4, TP7), T_avg_middle for sensors located at the middle (TP2, TP5, TP8), and T_avg_bottom for sensors located at the bottom (TP3, TP6, TP9). Fig. 5b shows that the energy stored in the module, estimated using the discrete volume approach (E_Finite volume), and the energy calculated using the law of energy conservation (E_Conservation law) have a high degree of agreement, with a zero-bias error of 2%. In the whole process, as observed in Fig. 5c, the energy in the module is mostly stored in the PCM accounting for more than 54% of the total energy stored, followed by aluminium with 29%, and lastly in the HTF in the module with 17%. The fact that the PCM accounts for more than half of the total energy, despite accounting for only 13% of the total mass of the module, is explained by its higher thermal energy density of 157.62 $kJ\cdot kg^{-1}$, as compared to 15.37 $kJ\cdot kg^{-1}$ of the aluminium and 56.32 $kJ\cdot kg^{-1}$ of the HTF.

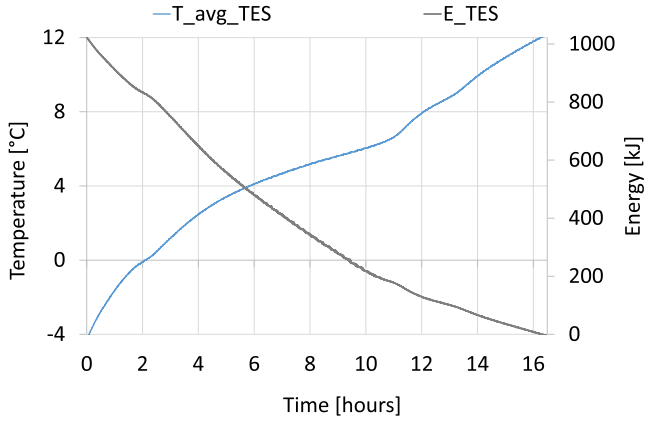

Fig. 4. Heat loss test to experimentally estimate the UA value of the evaporator-TES module.

At least three experiments were performed to ensure the repeatability of the experiments. Fig. 6 exemplifies the repeatability of the experimental measurements based on the average temperature of the PCM for three experiments at the same conditions. A high degree of repeatability is evident from the figure, whereby a maximum standard deviation of 0.65, 0.73, and 1.03 was observed for the average temperature at the top, middle, and bottom for the three experiments respectively.

3.3. Results of the charging tests

Fig. 7a shows the temperature evolution in the charging process (Case 1 in Table 2) with a constant energy source (compressor power at 30%) without energy demand (HTF flow rate equal to zero), while Fig. 7b presents the temperature evolution in a charging process accompanied with external energy demand. In both cases, the process starts with the module at (12 ± 0.5) °C, the refrigerant enters as a liquid–vapour mixture at the lowest temperature value and evaporates inside the module to attain a superheating value of about 5 °C as it leaves the module. As seen in Fig. 7a, the PCM at the bottom of the module charges faster achieving a temperature value around the refrigerant outlet temperature, while the PCM at the middle and top parts charges slower and never reaches a temperature value close to the refrigerant outlet temperature. This temperature stratification can be explained by the uneven distribution of the refrigerant which was mostly deposited at the bottom part of the module due to the higher density of the liquid fraction. As a result, most of the evaporation took place in the channels located at the bottom part of the module. In the course of the charging process, both the temperature in the module and refrigerant kept on lowering, and when the security set-point temperature −18 °C was attained, the condensing unit stopped. In the second case presented in Fig. 7b, the HTF enters the module at 12 °C and 100 $L\cdot h^{-1}$ and transfers heat to both the PCM and the refrigerant inside the module to cool down to around 5 °C as it leaves the module when steady-state conditions are attained. Contrary to the first case, the module maintains a constant temperature distribution at thermal equilibrium, and the minimum set-point temperature was not achieved allowing continuous heat exchange between the energy source and energy demand circuits.

Fig. 8a shows the energy stored in the module, the charging power of the PCM, the charging power of the sensible material (i.e. aluminium and HTF in the module), and the charging power of the whole module for the charging process, while Fig. 8b shows the energy stored in the

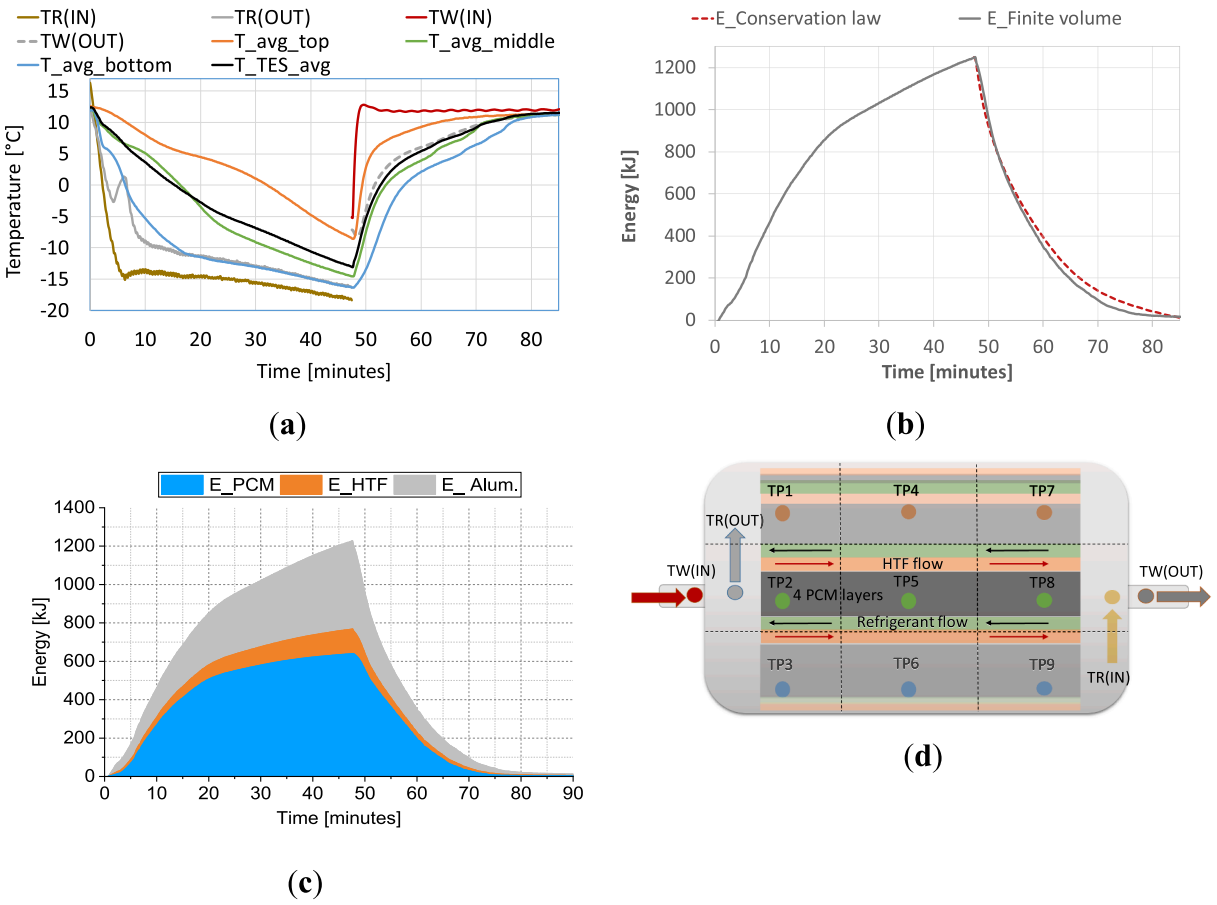

Fig. 5. Charging (compressor power 25%) with an immediate discharging process (HTF at 12 °C, 100 L·h^{-1}); (a) temperature evolution (b) validity of the discrete volume approach, (c) energy contribution in each material, and (d) position of temperature sensors.

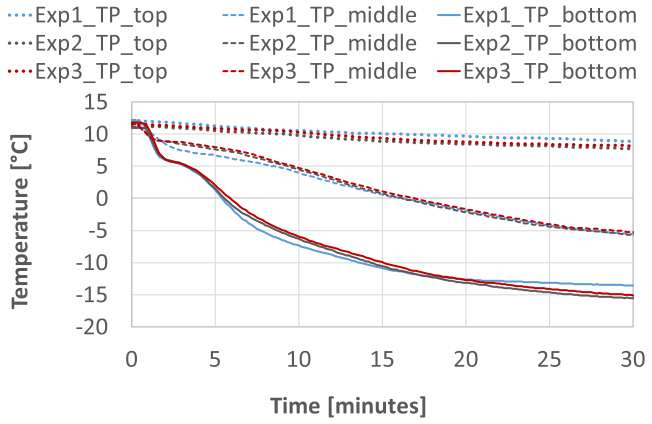

Fig. 6. Repeatability in temperature evolution in the PCM.

module, the overall charging power and the power delivered to the HTF loop during the three-fluids HEX mode of operation. As observed in Fig. 8a, the charging process took 40 min to reach the lower limit of safety conditions, while accumulating about 1350 kJ into the module. During the first 20 min, more than 1000 kJ was accumulated in the module, which is around three times the energy accumulated in the last 20 min of the process. Moreover, from the same figure, a higher charging power of the module can be observed in the first 20 min, with two peaks of the charging power. The first peak is due to the contribution of the sensible part of the energy stored in the module, which reached a maximum after around two minutes due to a rapid variation of the average temperature during this interval (Fig. 7a). After this initial period, most parts of the module reached a temperature near the PCM solidification point, when the average temperature slowed down its variation. As a consequence, the power corresponding to the sensible energy rapidly decreased, and a second peak was observed, which mostly corresponds to the energy variation of the latent part (PCM), as can be seen in Fig. 8a after around five minutes. Finally, most of the PCM underwent phase change after around 15 min, and the charging power experienced a sudden decrease after which it stabilized at around 300 W. In Fig. 8b the cold energy from the refrigerant loop was given simultaneously to the HTF loop and the module, as the module charging power decreased to zero, the HTF power increased to a maximum stable value when the thermal equilibrium was attained. By the time the thermal equilibrium was achieved, about 750 kJ was stored in the module while operating as a heat exchanger, whereby all the thermal power delivered by the refrigeration circuit was transferred to the HTF.

3.4. Results of the discharging tests

Fig. 7a shows the temperature evolution in the discharging process (Case 2 in Table 2) with a constant energy demand and without an external energy source, while Fig. 9b presents the temperature evolution in the discharging process accompanied by an external energy source. In the first case, the discharging process is accomplished by passing the HTF through the module constantly at 12 °C and 100 L·h^{-1} to discharge the cold energy stored in the module from −4 °C to 12 °C. The phase change is observed to start from the PCM at the top, followed by the middle and finally the bottom parts of the module. The temperature at the top layer went above the phase change temperature, 5 °C, after the first five minutes, while for the middle and bottom parts it occurred after

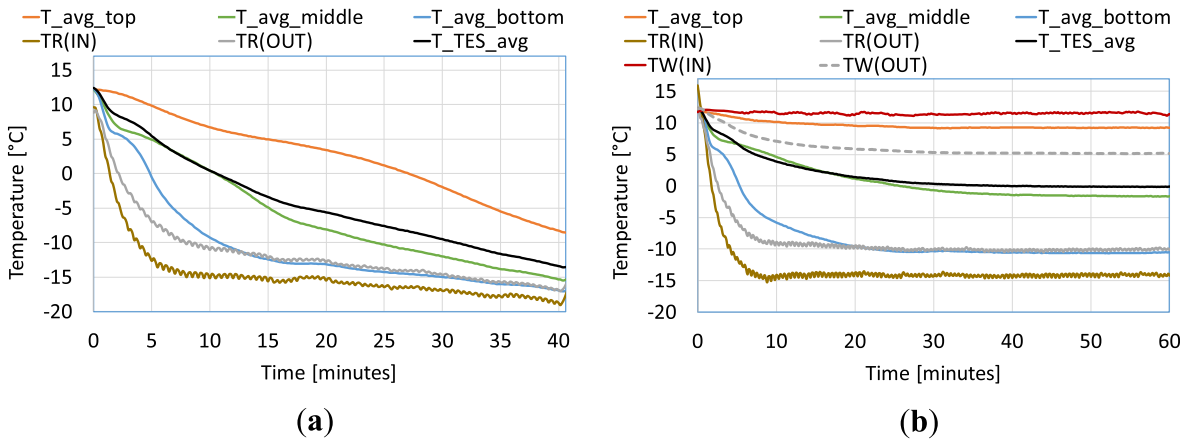

Fig. 7. Temperature evolution during charging process with compressor power at 30% (a) without external energy demand and (b) with external energy demand, i.e. HTF flow at 12 °C and 100 L·h^{-1}.

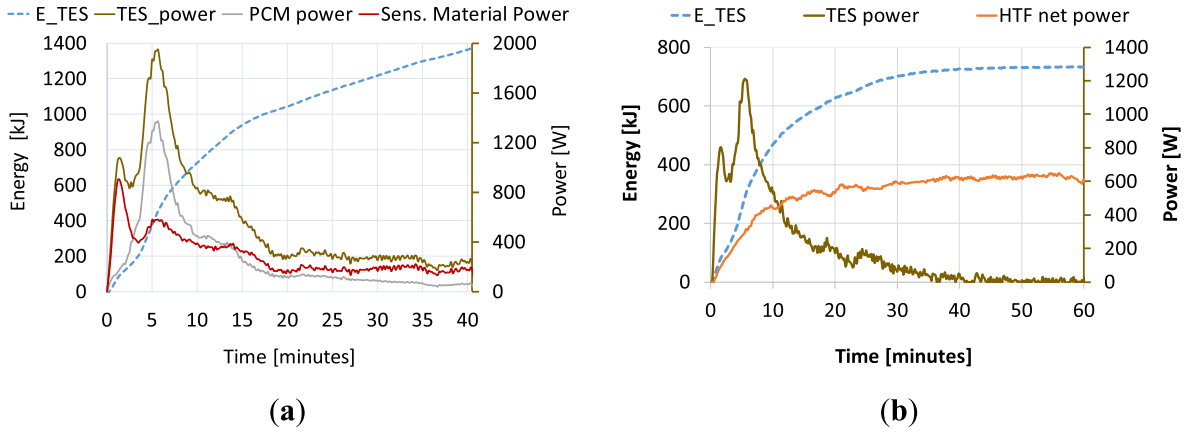

Fig. 8. Energy stored and power evolution during the charging process with compressor power at 30% (a) without external energy demand and (b) with external energy demand, i.e. HTF flow at 12 °C and 100 L·h^{-1}.

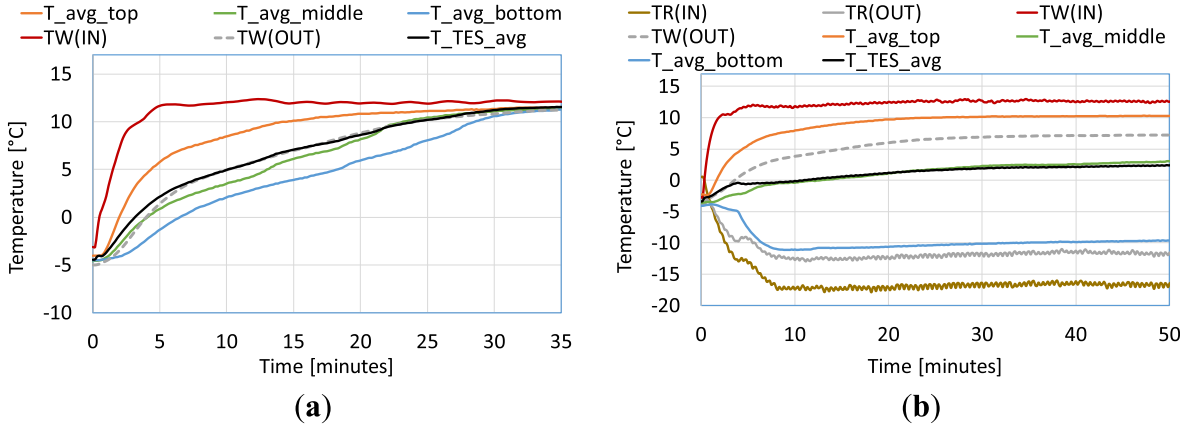

Fig. 9. Temperature evolution during discharging process with HTF flow at 12 °C and 100 L·h^{-1} (a) without external energy source and (b) with an external energy source, i.e. compressor power at 30%.

17 min and 20 min, respectively. As observed in the same figure, the HTF outlet temperature was close to the average temperature of the module, which brings out a better distribution of the HTF in the process than the refrigerant distribution as observed previously in Fig. 7a. The second case, in which both the HTF and the refrigerant flow through the module, is presented in Fig. 9b. The refrigerant entered at the lowest temperature value, and it is observed to further charge the PCM at the bottom part of the module before leaving the module with a degree of superheating of 5 °C. In the same figure, the HTF is observed to enter at 12 °C, taking cold from the module and the refrigerant, and leaving the module at a lower temperature value around 7 °C. In the process, the HTF slightly discharges the module at the middle part while mostly discharging it at the top by increasing its temperature to above 10 °C. When thermal equilibrium was attained, the temperature of the module

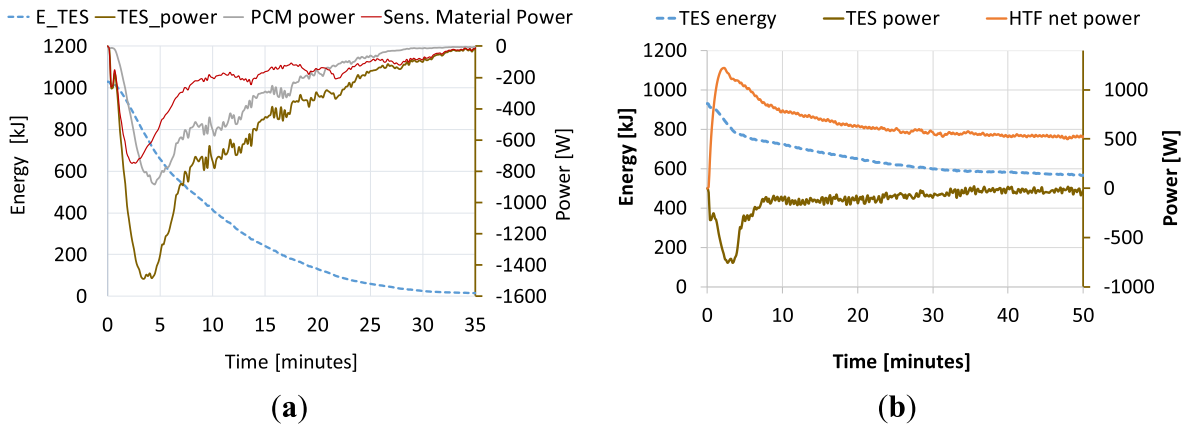

Fig. 10. Energy stored and power evolution during the discharging process with HTF flow at 12 °C and 100 L·h^{-1} (a) without external energy source and (b) with an external energy source, i.e. compressor power at 30%.

in the part between the middle and the bottom parts remained lower than the HTF outlet temperature, which means that, in case the refrigerant loop stopped, the HTF could take advantage of this lower temperature region to cover part of the energy demand.

Fig. 10 presents the energy stored in the module and the power transferred to both the PCM and the module during the discharging process for two situations, i.e. discharging the module without and with an external energy source. For both cases, the process started with the module completely charged with around 1000 kJ of cold energy. In the first case, as presented in Fig. 10a, the energy level in the module decreased with time until a complete discharge was achieved after 35 min. The discharging process was observed to be more effective in the first half of the discharging period, whereby around 85% of the total energy was discharged. Moreover, the rate of energy discharge of the module is observed to be highest within the first seven minutes, with a peak of almost 1500 W after five minutes. This peak can be attributed mainly to the discharging of the latent energy from the PCM, which is evident from the coincidence of the peaks of the PCM and the whole module discharging power.

For the second case, as observed in Fig. 10b, the HTF took cold energy simultaneously from the module and the refrigerant loop. The energy level in the module decreased from an initial value of 1000 kJ to 600 kJ at thermal equilibrium, thereafter maintaining this value constant since the module acts as a heat exchanger. The energy maintained in the module at thermal equilibrium could further be discharged to the HTF loop, in case the refrigerant loop was closed. Moreover, in this case, the module discharging power is observed to be more pronounced in the first 8 min, which is the time it took for the PCM at the top to completely phase change (Fig. 9b). As the HTF absorbs cold energy simultaneously from the module and from the refrigerant loop, the peak of the HTF net power is attributed to the peak of the discharging power of the module. As the module discharging power decreased towards zero, the HTF net power approached a constant value attributed only to the refrigerant net power.

3.5. Summary of the results and discussion

To perform a holistic analysis of the results obtained under different boundary conditions, Fig. 11 shows a summary of the energy level in the module and the HTF power during steady-state operating conditions, i.e. when the module acts as a heat exchanger. On the one hand, Fig. 11a shows the influence of the energy source (i.e. varying the compressor power) at a constant HTF flow rate of 100 L·h^{-1} on both the energy level in the module and the HTF power. In terms of energy stored in the module, it is directly affected by the compressor power, i.e. increasing the power of the energy source increases the energy level in the module, especially at lower compressor powers. In terms of power delivered to the HTF, the trend is similar, although in this case, the HTF power increases linearly with the compressor power in the whole range, as expected. On the other hand, Fig. 11b, shows the influence of the energy demand (i.e. varying the HTF flow rate) on both the energy level in the module and the HTF power for constant energy source (i.e. compressor power of 30%). In this case, at higher HTF flow rates, less energy is stored in the module, especially at a flow rate of 150 L·h^{-1} for which the value is significantly lower than the value corresponding to an HTF flow rate of 100 L·h^{-1}. In terms of power delivered to the HTF, a slight

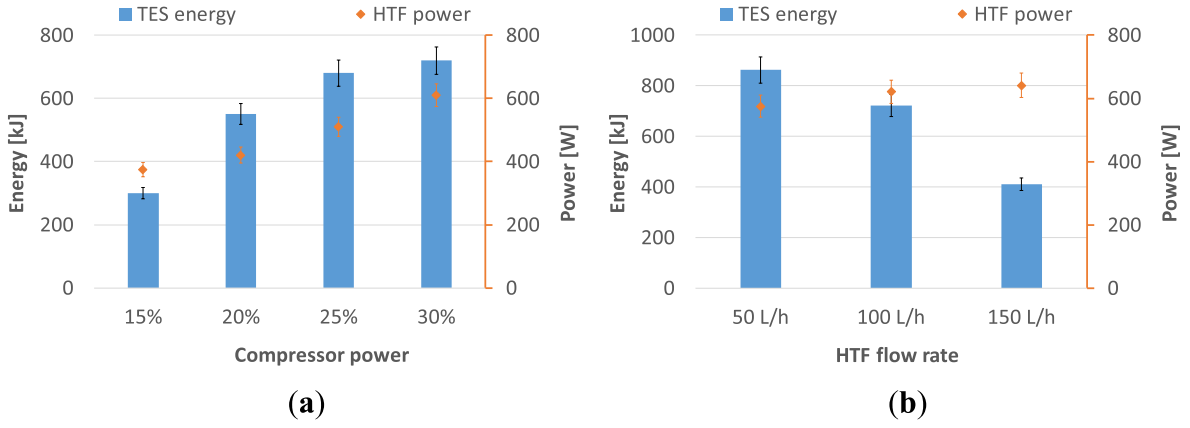

Fig. 11. The energy and HTF power at the thermal equilibrium for (a) different energy source levels, i.e. different compressor powers, and (b) different energy demand levels, i.e. HTF flow rates.

increase is observed when increasing the HTF flow rate.

Given the results shown in Fig. 11, one can argue that, in steady-state conditions, the module acts as a standard heat exchanger in terms of power transferred to the HTF, which increases linearly with the increase in the energy source (i.e. compressor power). It is worth highlighting that, although the compressor power is kept constant (30% of its maximum), the power transferred to the HTF is slightly higher for higher HTF flow rates, meaning that the net cooling power also increases, probably due to improved energy efficiency of the condensing unit.

However, the results can be of great relevance if the system operates under unsteady conditions, i.e. either with a variable energy source or variable energy demand. With a standard heat exchanger, if a fluctuation in the energy source occurred for a relatively short time, such as compressor shutdown or power increase for some reason, this would have a direct effect on the power transferred to the HTF, which may destabilise the demand side of the system. However, using the module investigated in this paper, because of the capability to store energy while acting as a heat exchanger, a sudden fluctuation in the energy source can be dampened by the thermal inertia of the module, compensating the lack or excess of energy source power with energy discharged from or charged to the module. As an example, if the compressor power reduced from 30% to 15%, the power transferred to the HTF would decrease from more than 600 W to less than 400 W. However, this decrease in the HTF power would not be instantaneous, because the reduction in the source power could be compensated by the power discharged from the module, which has the potential to partially discharge from around 700 kJ to around 300 kJ as seen in Fig. 11a.

If the fluctuation occurred in the energy demand side, i.e. by a sudden variation of the HTF flow rate, no significant HTF power variation would occur with a standard heat exchanger under constant energy source conditions. However, using the module studied in this paper, the change in the power required by the HTF circuit could be compensated by a change in the energy level of the module. As an example, if the HTF flow rate suddenly increased from 50 $L{\cdot}h^{-1}$ to 150 $L{\cdot}h^{-1}$ as a result of higher energy demand, the extra coolness required by the demand could come from a partial discharge of the module from more than 800 kJ to around 400 kJ, which could compensate for a limited period the lack of power available in the source circuit.

Furthermore, even for a constant energy source level and steady-state conditions, the suitable value of the HTF flow rate at a given time could depend on a target value for the energy level of the module capable of ensuring optimal system performance over a given period. Further investigation of this aspect is required to find an optimal control strategy of the module under given energy source and energy demand profiles, which is beyond the scope of this paper.

4. Conclusions

The current study presents a compact integration of PCM into a refrigeration system through modification of the evaporator. It involves testing a novel design of an evaporator that is filled with PCM between refrigerant and HTF channels. The channels are arranged in such a way to allow heat/cold exchange between the PCM, the refrigerant, and the HTF. An experimental campaign was carried out for different possible operations modes, i.e. charging, discharging, and three-fluids HEX mode. Detailed energy analysis was carried out and reported based on: the energy stored in each material, comparison between the three operation modes, the effective charging/discharging power during the process, and the key aspects to consider while using the novel evaporator. To ensure robustness and repeatability of the results, at least three repetitions were performed for each experiment, the uncertainty in the results was evaluated, and the effect of heat/cold loss was experimentally assessed and considered in the reported results.

The major conclusions driven from the study are as follows: a complete charging/discharging of the novel evaporator is feasible, while when it is performing as a heat exchanger (three-fluids HEX mode), thermal equilibrium is achieved at a point where the PCM is partially charged. The level of energy charged at thermal equilibrium strongly depends on the boundary conditions. This means that, for any intermittent condition of the energy demand or energy source, the module can respond to these changes by charging/discharging the PCM accordingly. The highest effective charging power occurred around the phase change temperature, i.e. when the average PCM temperature was between −2 °C and 7 °C. The highest portion of the total energy was stored in the PCM, accounting for 54% despite the PCM accounting for only 14% of the total weight. Indeed, this novel integration of PCM into the refrigeration system empowers the evaporator with a secondary benefit as latent energy storage apart from its primary function as a heat exchanger, but given the high stratification observed especially during the charging process, the user should be cautious to avoid the temperature of the HTF from dropping below its freezing temperature, which could lead to rupturing of the channels.

CRediT authorship contribution statement

Boniface Dominick Mselle: Conceptualization, Methodology, Formal analysis, Investigation, Writing – original draft, Visualization. **Gabriel Zsembinszki:** Conceptualization, Methodology, Formal analysis, Writing – original draft, Supervision. **David Vérez:** Formal analysis, Investigation, Writing – original draft, Visualization. **Emiliano Borri:** Writing – review & editing, Visualization. **Luisa F. Cabeza:** Conceptualization, Resources, Data curation, Writing – review & editing, Supervision, Project administration, Funding acquisition.

Declaration of Competing Interest

The authors declare that they have no known competing financial interests or personal relationships that could have appeared to influence the work reported in this paper.

Acknowledgements

This work was partially funded by the Ministerio de Ciencia, Innovación y Universidades de España (RTI2018-093849-B-C31 - MCIU/AEI/FEDER, UE) and by the Ministerio de Ciencia, Innovación y Universidades - Agencia Estatal de Investigación (AEI) (RED2018-102431-T). The authors would like to thank the Catalan Government for the quality accreditation given to their research group GREiA (2017 SGR 1537). GREiA is a certified agent TECNIO in the category of technology developers from the Government of Catalonia. This work is partially supported by ICREA under the ICREA Academia programme. Boniface Dominick Mselle would like to thank Programa Santander Predoc UdL for his research fellowship.

References

[1] International Energy Agency World Energy Outlook 2019; Paris, 2019.
[2] United nations framework convention on climate change Paris Agreement. Paris, Fr., 2015.
[3] L.F. Cabeza, D. Urge-Vorsatz, M.A. McNeil, C. Barreneche, S. Serrano, Investigating greenhouse challenge from growing trends of electricity consumption through home appliances in buildings, Renew. Sustain. Energy Rev. 36 (2014) 188–193.
[4] UN General Assembly Transforming our world : the 2030 agenda for sustainable development Available online: https://www.refworld.org/docid/57b6e3e44.html (accessed on Mar 17, 2020).
[5] B. Zalba, J.M. Marín, L.F. Cabeza, H. Mehling, Review on thermal energy storage with phase change: materials, heat transfer analysis and applications, Appl. Therm. Eng. 23 (2003) 251–283.
[6] H. Mehling, L.F. Cabeza, Heat and cold storage with PCM. An up to date introduction into basics and applications; 1st ed.; Springer-Verlag Berlin Heidelberg: Berlin, Germany, 2008; ISBN 979-3-540-68556-2.
[7] M. Mastani Joybari, F. Haghighat, J. Moffat, P. Sra, Heat and cold storage using phase change materials in domestic refrigeration systems: The state-of-the-art review, Energy Build. 106 (2015) 111–124.
[8] A. Pirvaram, S.M. Sadrameli, L. Abdolmaleki, A.R. Sivaram, K. Karuppasamy, R. Rajavel, B. Arun Prasad, M. Visek, C.M. Joppolo, L. Molinaroli, et al., Review on

phase change materials (PCMs) for cold thermal energy storage applications, Int. J. Refrig. 35 (2017) 984–991.
[9] B.D. Mselle, G. Zsembinszki, E. Borri, D. Vérez, L.F. Cabeza, Trends and future perspectives on the integration of phase change materials in heat exchangers, J. Energy Storage (2021).
[10] M. Medrano, M.O. Yilmaz, M. Nogués, I. Martorell, J. Roca, L.F. Cabeza, Experimental evaluation of commercial heat exchangers for use as PCM thermal storage systems, Appl. Energy 86 (2009) 2047–2055.
[11] Jaume Gasia, Laia Miró, Alvaro de Gracia, Camila Barreneche, Luisa Cabeza, Experimental evaluation of a paraffin as phase change material for thermal energy storage in laboratory equipment and in a shell-and-tube heat exchanger, Appl. Sci. 6 (4) (2016) 112, https://doi.org/10.3390/app6040112.
[12] G. Zsembinszki, C. Orozco, J. Gasia, T. Barz, J. Emhofer, L.F. Cabeza, Evaluation of the State of Charge of a Solid/Liquid Storage Tank, Energies 13 (1425) (2020) 1–26.
[13] J. Emhofer, K. Marx, T. Barz, F. Hochwallner, L.F. Cabeza, G. Zsembinszki, A. Strehlow, B. Nitsch, M. Wiesflecker, W. Pink, Techno-economic analysis of a heat pump cycle including a three-media refrigerant/phase change material/water heat exchanger in the hot superheated section for efficient domestic hot water generation, Appl. Sci. 10 (2020) 7873.
[14] E. Varvagiannis, A. Charalampidis, G. Zsembinszki, S. Karellas, L.F. Cabeza, Energy assessment based on semi-dynamic modelling of a photovoltaic driven vapour compression chiller using phase change materials for cold energy storage, Renew. Energy 163 (2021) 198–212.
[15] B.D. Mselle, D. Vérez, G. Zsembinszki, E. Borri, L.F. Cabeza, Performance Study of Direct Integration of Phase Change Material into an Innovative Evaporator of a Simple Vapour Compression System, Appl. Sci. 10 (2020) 4649.
[16] Rubitherm Rubitherm RT-LINE Datasheet.
[17] G. Zsembinszki, A.G. Fernández, L.F. Cabeza, Selection of the appropriate phase change material for two innovative compact energy storage systems in residential buildings, Appl. Sci. 10 (2020), 2116-1-2116–14.
[18] G. Ferrer, C. Barreneche, A. Solé, I. Martorell, L.F. Cabeza, New proposed methodology for specific heat capacity determination of materials for thermal energy storage (TES) by DSC, J. Energy Storage 11 (2017) 1–6.
[19] The Dow Chemical Company Dowtherm SR-1.
[20] J. Carvill, Thermodynamics and heat transfer, in: Mechanical Engineer's Data Handbook, Elsevier, 1993, pp. 102–145.
[21] M. Fang, G. Chen, Effects of different multiple PCMs on the performance of a latent thermal energy storage system, Appl. Therm. Eng. 27 (2007) 994–1000.
[22] Amin Ebrahimi, Chris R. Kleijn, Ian M. Richardson, Sensitivity of numerical predictions to the permeability coefficient in simulations of melting and solidification using the enthalpy-porosity method, Energies 12 (22) (2019) 4360, https://doi.org/10.3390/en12224360.
[23] V.R. Voller, Fast implicit finite-difference method for the analysis of phase change problems, Numer. Heat Transf. Part B Fundam. 17 (1990) 155–169.
[24] Y.A. Cengel, M.A. Boles, Thermodynamics: An Engineering Approach, 7th ed., McGraw-Hill, New York, NY, USA, 2010.
[25] P. Eames, Applied Thermal Engineering Experimental evaluation of the use of reversible heat pipes as heat transfer enhancement technique versus a conventional shell and tubes heat exchanger for more compact latent heat thermal energy storage systems, 2021.
[26] J.C. Gomez, G.C. Glatzmaier, M. Mehos, Heat Capacity Uncertainty Calculation for the Eutectic Mixture of Biphenyl/Diphenyl Ether Used as Heat Transfer Fluid, Prepr. Present. SolarPACES 2012, Marrakech (Morocco), Sept. 11–14, 2012, 2012.
[27] Joint Committee for Guides in Metrology (JCGM) Guide to the expression of uncertainty in measurement — Part 6: Developing and using measurement models. **2020**.
[28] E.O. Dahl, K.-E. Frøysa, P. Lunde, Handbook of Uncertainty Calculations. Fiscal Orifice Gas and Turbine Oil Metering Stations, 2003; ISBN 8291341621.